All-Polymer Solar Cells

International Edition: DOI: 10.1002/anie.201807513
German Edition: DOI: 10.1002/ange.201807513

Highly Flexible and Efficient All-Polymer Solar Cells with High-Viscosity Processing Polymer Additive toward Potential of Stretchable Devices

Shanshan Chen[+], Sungwoo Jung[+], Hye Jin Cho[+], Na-Hyang Kim, Seungon Jung, Jianqiu Xu, Jiyeon Oh, Yongjoon Cho, Hyeongwon Kim, Byongkyu Lee, Yujin An, Chunfeng Zhang, Min Xiao, Hyungson Ki, Zhi-Guo Zhang, Ju-Young Kim, Yongfang Li, Hyesung Park, and Changduk Yang**

Abstract: *Considering the potential applications of all-polymer solar cells (all-PSCs) as wearable power generators, there is an urgent need to develop photoactive layers that possess intrinsic mechanical endurance, while maintaining a high power-conversion efficiency (PCE).Herein a strategy is demonstrated to simultaneously control the intercalation behavior and nanocrystallite size in the polymer–polymer blend by using a newly developed, high-viscosity polymeric additive, poly(dimethylsiloxane-co-methyl phenethylsiloxane) (PDPS), into the TQ-F:N2200 all-PSC matrix. A mechanically robust 10wt% PDPS blend film with a great toughness was obtained. Our results provide a feasible route for producing high-performance ductile all-PSCs, which can potentially be used to realize stretchable all-PSCs as a linchpin of next-generation electronics.*

Compared with small-molecule-containing organic solar cells, all-polymer solar cells (all-PSCs), comprising polymeric donor and acceptor, inherently have better solution processability and mechanical robustness, which are necessary for cost-effective flexible and wearable devices that are produced by printing technologies.[1] While intensive efforts have focused on maximizing the performances of the all-PSCs through the design of new materials and optimal combinations in blends, yielding impressive power-conversion efficiencies (PCEs) over 7% within a short time, there are at present few studies that have realized the viability of all-PSCs with mechanical stability toward the aforementioned next-generation electronics.[1d,2] The mechanical compliance of π-conjugated polymers can be enhanced through the incorporation of soft segments within the backbone.[3] However, these approaches not only suppress molecular packing in the condensed phase, but also reduce the density of chromophores in the π-conjugated polymer, resulting in a massive decrease of the inherent electrical properties.[4] To surmount such incompatibilities between the photovoltaic and mechanical properties of semiconductors, several blending methods using rubber-like plasticizers or elastic polymers were explored.[3a,b,4a,5] Besides, we confirmed that using polymeric additives can help refine bulk heterojunction (BHJ) morphology in blend and enhance the PCE.[6] Therefore, we hypothesized that a processing polymer additive with high viscosity can provide an effective simultaneous control over mechanical and photovoltaic properties in all-PSC.

In this work, we have synthesized a high-viscosity hydrophobic polymer, poly(dimethylsiloxane-*co*-methyl phenethylsiloxane) (PDPS), by grafting styrene to hydrosilane-terminated poly(dimethylsiloxane-*co*-methylhydrosiloxane) (PDMS), showing approximately a fourfold enhancement in viscosity over that of PDMS (Figure 1).[7] We have investigated the effects of PDPS as an additive on the mechanical properties, morphology, and photovoltaic characteristics of all-PSC platforms based on the poly(6-fluoro-2,3-bis-(3-octyloxyphenyl)quinoxaline-5,8-dyl-*alt*-thiophene-2,5-diyl) (TQ-F):poly((*N*,*N*′-bis(2-octyldodecyl)-naphthalene-1,4,5,8-bis(dicarboximide)-2,6-diyl)-*alt*-5,5′-(2,2′-bithiophene)) (P(NDI2OD-T2, known as N2200) matrix.[2f] Upon addition of 10 wt% PDPS into the polymeric matrix, the resulting

[*] S. Chen,[+] S. Jung,[+] H. J. Cho,[+] S. Jung, J. Oh, Y. Cho, B. Lee, Y. An, Prof. H. Park, Prof. C. Yang
Department of Energy Engineering, School of Energy and Chemical Engineering, Perovtronics Research Center, Low Dimensional Carbon Materials Center, Ulsan National Institute of Science and Technology (UNIST)
50 UNIST-gil, Ulju-gun, Ulsan 44919 (South Korea),
E-mail: yang@unist.ac.kr
hspark@unist.ac.kr
N.-H. Kim, Prof. J.-Y. Kim
School of Materials Science and Engineering, Ulsan National Institute of Science and Technology (UNIST)
50 UNIST-gil, Ulju-gun, Ulsan 44919 (South Korea)
J. Xu, Prof. C. Zhang, Prof. M. Xiao
National Laboratory of Solid State Microstructures, School of Physics, and Collaborative Innovation Center of Advanced Microstructures, Nanjing University
Nanjing 210093 (China)
H. Kim, Prof. H. Ki
School of Mechanical and Nuclear Engineering, Ulsan National Institute of Science and Technology (UNIST)
50 UNIST-gil, Ulju-gun, Ulsan 44919 (South Korea)
Prof. Z.-G. Zhang, Prof. Y. Li
Beijing National Laboratory for Molecular Sciences, CAS Key Laboratory of Organic Solids, Institute of Chemistry, Chinese Academy of Sciences
Beijing 100190 (China)
[+] These authors contributed equally to this work.
Supporting information and the ORCID identification number(s) for the author(s) of this article can be found under: https://doi.org/10.1002/anie.201807513.

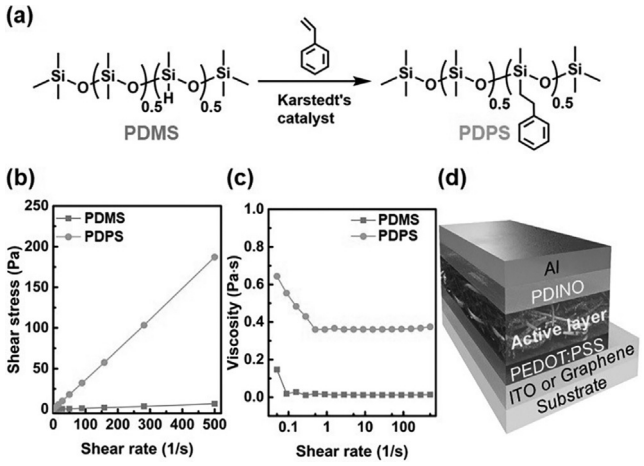

Figure 1. a) Synthetic route for PDPS. b) Dependence of shear stress and c) dynamic viscosities of PDMS and PDPS on the shear rate at 25 °C, respectively. d) Diagram of the conventional all-PSCs with the configuration of substrate (glass or PET)/ ITO or graphene/active layer (TQ-F:N2200:PDPS)/PDINO/Al.

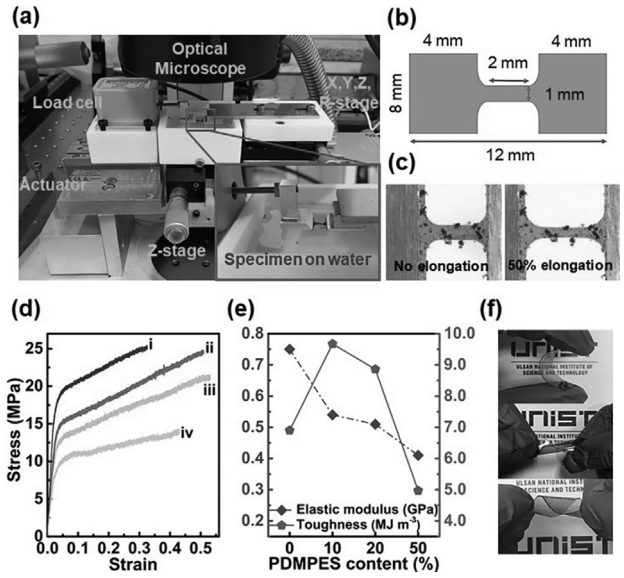

Figure 2. a) The pseudo free-standing tensile test system. b) The dog-bone-shaped tensile specimen used in this work. c) Optical microscopy images of the representative 10PDPS blend film under different strains. d) The strain-stress curves and e) corresponding elastic modulus and integrated toughness values of the (i) 0PDPS, (ii) 10PDPS, (iii) 20PDPS, (iv) 50PDPS blend films. f) The blend films deposited on the PET substrate, bent at various configurations.

blend film exhibits superior toughness values of up to 9.67 MJ m^{-3} with a elongation at a break of 50.92 %. This allows achieving not only a high PCE of 6.87 % in conventional all-PSCs but also a reliable PCE of 5.60 % in graphene electrode-based flexible devices, for which 90 % of its PCE is retained after 100 bending cycles at a bending radius of 3 mm. The present work demonstrates a simple processing route to potentially produce highly efficient stretchable photoactive layers for wearable all-PSCs.

A pseudo free-standing tensile test system (Figure 2 a) was employed to measure the intrinsic mechanical properties of the blend films.[1d,8] The blend films incorporated with varying amounts of PDPS (0, 10, 20, and 50 wt %) relative to the total weight of the photoactive layer are denoted as 0PDPS, 10PDPS, 20PDPS, and 50PDPS, respectively.

The elastic modulus, elongation at break, and integrated toughness of the 0PDPS film were 0.75 GPa, 32.56 %, and 6.90 MJ m^{-3}, respectively. The addition of 10 wt % PDPS into the TQ-F:N2200 matrix retains a comparable tensile strength of 24.62 MPa, but significantly lowers the elastic modulus to 0.54 GPa with a greatly enhanced elongation at a break of 50.92 %, thereby yielding a high toughness value of 9.67 MJ m^{-3} (Figure 2 d and e). The detailed data are summarized in Table S1 in the Supporting Information. No cracks until the high elongation of up to 50 %, was observed in the representative 10PDPS film (Figure 2 c). The storage (G') and loss (G'') moduli of the blend films show a weak dependence on the frequency, where the G' values were higher than those of the corresponding G'' over the measured frequency range (Figure S4, see the Supporting Information), indicating typical gel-type behavior. It is also noted that both G' and G'' moduli increase with increasing the PDPS content. The superior ductile nature is a crucial advantage for stretchable electronic applications. Further increase of the PDPS contents leads to a monotonic decrease in both elastic modulus and tensile strength, while the elongations at the break are 53.15 % and 42.96 % in the 20PDPS and the 50PDPS, respectively, resulting in an overall decrease in toughness values in both cases (Figure 2 d and e). This suggests that adding an optimal amount of PDPS into the BHJ blend helps maximize the mechanical endurance. Additionally, we fabricated the 10PDPS film on the polyethylene terephthalate (PET) substrate, confirming its outstanding mechanical durability (Figure 2 f).

Conventional all-PSCs with the configuration of indium tin oxide (ITO)/poly(3,4-ethylenedioxythiophene): poly(styrenesulfonate) (PEDOT:PSS)/TQ-F:N2200:PDPS/perylenediimide functionalized with amino *N*-oxide (PDINO)/Al were fabricated. All active layers were optimized to be around 110 nm for the sake of comparison. Figure 3 a shows the representative curves of current density–voltage (J–V) measured under an AM 1.5 G condition, 100 W cm^{-2}, and the relevant photovoltaic parameters are summarized in Figure 3 b and Table S2 in the Supporting Information. Figure 3 c displays the external quantum efficiency (EQE) spectra of all devices, and the corresponding integrated J_{SC} values (Figure 3 d) agree with the J_{SC} values obtained from the J–V measurement (within 5 % mismatch). The 0PDPS-based cell exhibited a PCE of 7.12 % with a short-circuit current density (J_{SC}) of 13.58 mA cm^{-2}, open-circuit voltage (V_{OC}) of 0.841 V, and fill factor (FF) of 62.33 %, consistent with the values reported.[2f] Upon adding PDPS, the J_{SC} values drop gradually while maintaining similar V_{OC} values of about 0.82–0.84 V. Notably, the addition of 10 wt % PDPS provides an unexpected high FF of 65.96 %, together with only a minimal decrease in J_{SC} (12.40 mA cm^{-2}), yielding a high PCE of 6.87 %, comparable to the PDPS-free one. However, at higher PDPS loadings (20 and 50 wt %), additionally to the further decrease in J_{SC} values, the FF values decline sharply, leading

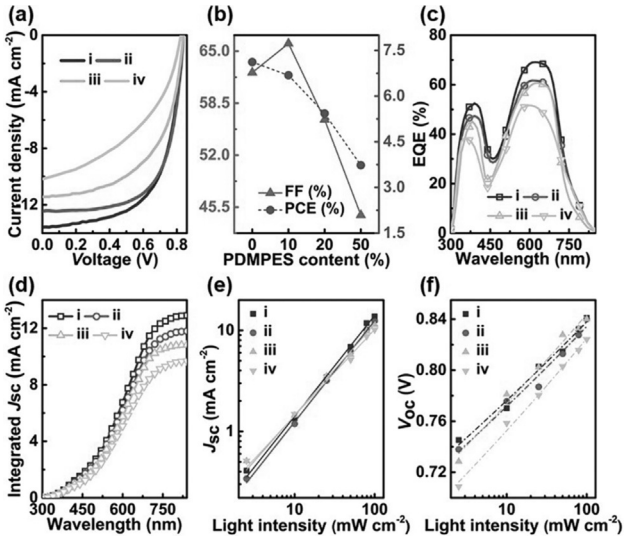

Figure 3. a) The current density–voltage (*J–V*) curves of (i) 0PDPS, (ii) 10PDPS, (iii) 20PDPS, (iv) 50PDPS blend films. b) PDPS content dependence in FF and PCE parameters from devices as described in (a). c) Corresponding EQE spectra; d) integrated J_{SC} values; e) dependence of $J_{SC,}$ and f) V_{OC} as a function of light intensity.

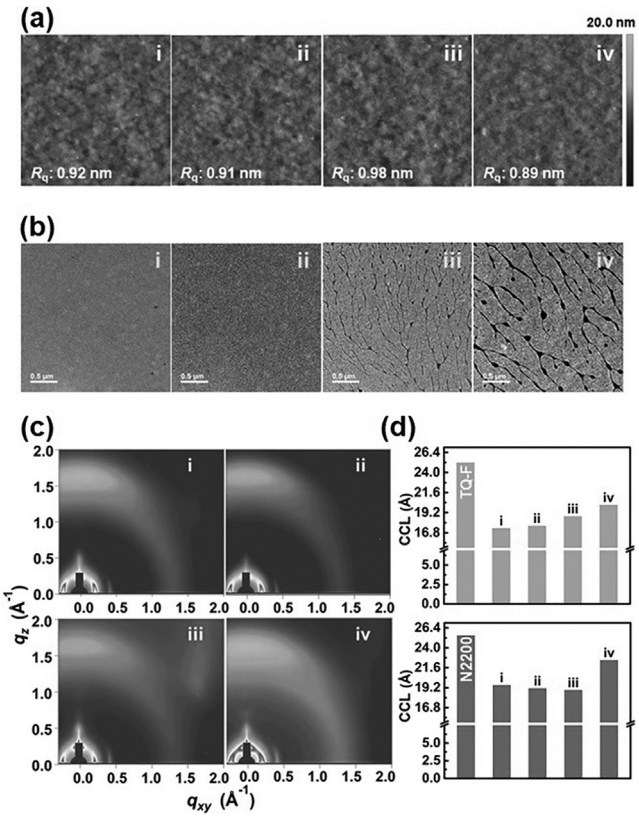

Figure 4. a) AFM height images in 4 μm × 4 μm, b) TEM images, and c) GIWAXS images of the blend films: (i) 0PDPS, (ii) 10PDPS, (iii) 20PDPS, (iv) 50PDPS. d) Corresponding donor and acceptor components coherence lengths (CCLs) estimated from the face-on (010) diffractions.

to a low power output in the devices. Comprehensively, the 10PDPS blend possessing superior mechanical and photovoltaic properties facilitate the realization of a high-performance PSC with stretchable features.

To understand the correlation between the PDPS content and the mechanical and photovoltaic performance difference, atomic force microscopy (AFM) and bright-field transmission electron microscopy (TEM) were used to probe the top surface and bulk features of the blend films, respectively. (Figure 4a and b) All AFM images of the blend films exhibit a similar smooth surface with a low root-mean-square roughness in the range of 0.89–0.98 nm. Whereas the TEM images clearly reveal that varying PDPS contents in the blends significantly affects the degree of phase separation. For example, the TEM image of PDPS-free blend film shows only a homogeneous and smooth feature, while fibril-like microstructures are clearly seen from the blend film with a 10 wt % PDPS, indicating phase-separated polymer networks. Such a fibril-like feature could be strongly related with change in the interfacial tension induced by the addition of PDPS (see the tension analysis among each configuration in Figure S7 and Table S3, see the Supporting Information).This type of morphology is expected to not only enhance the mechanical robustness, but also the charge transport. Both these enhancements can contribute positively to tensile and photovoltaic properties mentioned above.[1a–c,9,10] However, the TEM images of the blend films with more than 20 wt % PDPS present tree branch textures with poor film formation. This is probably due to the insufficient intermixing of PDPS with the photoactive layer polymers, which is responsible for the concomitant fall in J_{SC} and FF values in devices and reduced mechanical toughness as well. X-ray photoelectron spectroscopy (XPS) measurement was carried out to analyze the composition of 10PDPS film as a function of the penetration depth (Figure S8, see the Supporting Information), where the silicon (Si) and sulfur (S) atoms can be used as the characteristic elements of the PDPS and TQ-F:N2200 host matrix, respectively. The calculated Si:S ratio showed a close correlation with the penetration depth of blend film according to the etching time, suggesting that the degree of the PDPS dispersion is evidently different between the surface and the bulk regions of the blend film. This result support the observed discrepancy in the AFM and TEM results.

Moreover, a deeper insight into the molecular packing and orientation of the blend films was obtained through grazing incident wide-angle X-ray scattering (GIWAXS) measurement. As shown in Figure 4c and Figure S10 in the Supporting Information, all the blend films with and without PDPS yielded strong (010) π–π stacking diffraction along the out-of-plane, that is, the so-called π-face-on orientation, benefitting the charge transfer through photoactive layer to electrodes.[11] The different (010) diffraction positions of neat TQ-F (Ca. 1.71 Å^{-1}) and N2200 (Ca. 1.57 Å^{-1}) allows us to resolve the corresponding (010) π-face-on peaks in blend films by multiple-peak fitting (Figure S9 and S11,see the Supporting Information). Calculated by Scherrer's equation, the crystallite coherence lengths (CCLs) in blend films are smaller than the corresponding neat films.[12] Noted that the CCLs in blend films arising from the TQ-F polymer gradually increase from 17.34 Å to 20.12 Å with increasing PDPS content, though no monotonic trend in the CCLs of the N2200

polymer was observed (Figure 4d). The results demonstrate that the incorporation of PDPS into the polymer blend matrix affects the molecular packing and nanocrystallite sizes in both the polymeric components, rather than the molecular orientation. Considering the above morphological studies, one can speculate that the well-modulated nanocrystallite sizes of both donor and acceptor polymers with phase-separated networks in the blend films increase the intercalation and interface area between the two polymer components.[2e,13]

To directly compare the vertical bulk charge transport properties of the blends, space-charge-limited current (SCLC) measurements were performed.[14] As shown in Figure S12 in the Supporting Information, the estimated hole mobilities (μ_h) exhibit the following order: 50PDPS (1.91×10^{-5} $cm^2V^{-1}s^{-1}$) < 20PDPS (5.40×10^{-5} $cm^2V^{-1}s^{-1}$) < 0PDPS (8.25×10^{-5} $cm^2V^{-1}s^{-1}$) < 10PDPS (9.37×10^{-5} $cm^2V^{-1}s^{-1}$). Moreover, we analyzed incident light-intensity (I) dependent J–V characteristics to further understand the charge recombination kinetics.[15,16] Figure 3e shows a log–log plot of J_{SC} as a function of I. The dependence characteristic of J_{SC} on I is used to determine the bimolecular recombination, which limits the FF output. A power-law function correlation is given by $J_{SC}\propto I^{\alpha}$, in which exponent $\alpha=1$ when the bimolecular recombination of the free carriers is negligible under the short-circuit condition.[15] The determined values of α were 0.99, 1.00, 0.90, and 0.85 for 0PDPS, 10PPES, 20PDPS, and 50PDPS, respectively, suggesting that the least bimolecular recombination loss was involved in the 10PDPS blend, unambiguously reflecting its highest FF value in all-PSCs. Besides, the geminate or Shockley–Read–Hall recombination loss was also extracted from the dependence of V_{OC} on I (Figure 3f).[15] The magnitude of the slope represents the degree of geminate recombination before the photoinduced excitons fully dissociate into free charge carriers. The slopes for 0PDPS, 10PDPS, 20PDPS, and 50PDPS were determined to be 1.28 kT/q, 1.30 kT/q, 1.45 kT/q, and 1.53 kT/q, respectively, indicating that the geminate recombination loss increases as the PDPS content increases in the blends, consistent with the observed J_{SC} trend above.

To investigate the effect of PDPS additive on the photoinduced charge transfer dynamics in all-PSCs, transient absorption (TA) measurement was performed on the 0PDPS and 10PDPS blend films, where the pump wavelengths at 500 nm and 740 nm were used to excite TQ-F and N2200, respectively (Figure S14–S17, see the Supporting Information). Clear hole and electron transfer processes were observed in both cases. Notably, with pump at 740 nm, the bi-exponential fitted rising lifetimes of excited-state absorption (ESA) signal probed at 860 nm, which was attributed to the hole transfer process, are 0.64 ps, 10.56 ps for 10PDPS and 0.77 ps, 13.15 ps for 0PDPS, respectively. On the other hand, with pump at 500 nm, the ESA rising lifetimes attributed to electron transfer process are 1.01 ps, 11.85 ps for 10PDPS and 1.47 ps, 14.42 ps for 0PDPS, respectively. These results suggest that the use of PDPS additive can facilitate the charge transfer kinetics, mainly due to the well-distributed microstructure with finer interconnected phase-separation in the 10PDPS, which accounts for its outstanding performance.

To further evaluate the stability of the photovoltaic properties against external mechanical deformation, we performed the bending test on 0PDPS and 10PDPS based flexible all-PSCs using the configuration of PET/graphene/PEDOT:PSS/active layer/PDINO/Al.[17] Their J–V characteristics were measured after different bending cycles at a bending radius of 3.0 mm. Note that a higher sheet resistance of the graphene electrode relative to that of ITO as well as the graphene transfer-related defects may account for the slightly inferior device performances observed from the flexible devices.[5d,17a,18] As shown in Figure 5a and Table S4 in the Supporting Information, although the 0PDPS afforded a higher PCE (5.89%) initially, both J_{SC} and FF dramatically

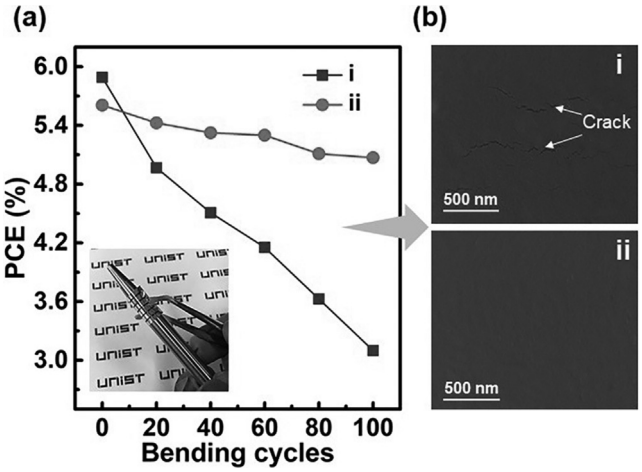

Figure 5. a) The PCEs of (i) 0PDPS and (ii) 10PDPS based flexible all-PSCs with bending cycles at a bending radius of 3 mm. b) Corresponding SEM images of surface morphologies of photoactive layer after 100 bending cycles.

degraded as the bending number increased, leading to significantly reduced PCE of only 3.10%, that is, a decrease of 50%, after 100 bending cycles. The apparent degradation of photovoltaic efficiencies was mostly attributed to crack propagation in the 0PDPS blend film under the bending strain (Figure 5b). In contrast, together with negligible morphological change, the device performance of 10PDPS was found to be much more stable while retaining a decent PCE of 5.07% at the same measurement conditions, that is, about 90% of its initial PCE (5.60%). The trend of bending test agrees well with the tensile modulus analysis mentioned previously, suggesting that the PDPS-assisted BHJ blend films provide excellent tolerance against external strains with stable photovoltaic performance.

In summary, we have developed a high-viscosity hydrophobic PDPS that has an approximately fourfold enhancement in viscosity by grafting reaction of styrene to the PDMS backbone and have applied it as a processing additive to the TQ-F:N2200-based all-PSCs. By properly controlling the PDPS content in the polymer-polymer matrix, a strong intercalated phase-separated network with desirably-controlled nanocrystallite sizes in blend films was observed in the 10PDPS, enabling high-performance all-PSCs with

mechanical durability. Besides, we also fabricated a graphene electrode-based flexible device with the best-performing 10PDPS blend, not only achieving a high PCE of 5.60%, but also maintaining 90% of the initial PCE after 100 bending cycles with a bending radius of 3.0 mm. Our study paves a simple yet feasible approach to manufacture efficient flexible all-PSCs and demonstrates its potential for high-performance stretchable all-PSCs as a cornerstone of portable and wearable devices.

Acknowledgements

This work was supported by the National Research Foundation of Korea (NRF) grant funded by the Korea government (MSIP) (**2018R1A2A1A05077194**) and the Center for Advanced Soft-Electronics funded by the Ministry of Science and ICT as Global Frontier Project (2012M3A6A5055225).

Conflict of interest

The authors declare no conflict of interest.

Keywords: all-polymer solar cells · flexibility · mechanical robustness · PDPS · polymer additive

How to cite: *Angew. Chem. Int. Ed.* **2018**, *57*, 13277 – 13282
Angew. Chem. **2018**, *130*, 13461 – 13466

[1] a) S. E. Root, S. Savagatrup, A. D. Printz, D. Rodriquez, D. J. Lipomi, *Chem. Rev.* **2017**, *117*, 6467 – 6499; b) S. Savagatrup, A. D. Printz, T. F. O'Connor, A. V. Zaretski, D. J. Lipomi, *Chem. Mater.* **2014**, *26*, 3028 – 3041; c) G.-J. N. Wang, A. Gasperini, Z. Bao, *Adv. Electron. Mater.* **2018**, *4*, 1700429; d) T. Kim, J. H. Kim, T. E. Kang, C. Lee, H. Kang, M. Shin, C. Wang, B. Ma, U. Jeong, T. S. Kim, B. J. Kim, *Nat. Commun.* **2015**, *6*, 8547 – 8554.

[2] a) H. Kang, W. Lee, J. Oh, T. Kim, C. Lee, B. J. Kim, *Acc. Chem. Res.* **2016**, *49*, 2424 – 2434; b) Z. G. Zhang, Y. Yang, J. Yao, L. Xue, S. Chen, X. Li, W. Morrison, C. Yang, Y. Li, *Angew. Chem. Int. Ed.* **2017**, *56*, 13503 – 13507; *Angew. Chem.* **2017**, *129*, 13688 – 13692; c) L. Gao, Z. G. Zhang, L. Xue, J. Min, J. Zhang, Z. Wei, Y. Li, *Adv. Mater.* **2016**, *28*, 1884 – 1890; d) B. Fan, L. Ying, Z. Wang, B. He, X.-F. Jiang, F. Huang, Y. Cao, *Energy Environ. Sci.* **2017**, *10*, 1243 – 1251; e) N. Zhou, A. S. Dudnik, T. I. Li, E. F. Manley, T. J. Aldrich, P. Guo, H. C. Liao, Z. Chen, L. X. Chen, R. P. Chang, A. Facchetti, M. Olvera de la Cruz, T. J. Marks, *J. Am. Chem. Soc.* **2016**, *138*, 1240 – 1251; f) S. Chen, Y. An, G. K. Dutta, Y. Kim, Z.-G. Zhang, Y. Li, C. Yang, *Adv. Funct. Mater.* **2017**, *27*, 1603564; g) B. Fan, L. Ying, P. Zhu, F. Pan, F. Liu, J. Chen, F. Huang, Y. Cao, *Adv. Mater.* **2017**, *29*, 1703906; h) Y. Guo, Y. Li, O. Awartani, J. Zhao, H. Han, H. Ade, D. Zhao, H. Yan, *Adv. Mater.* **2016**, *28*, 8483; i) J. W. Jung, J. W. Jo, C. C. Chueh, F. Liu, W. H. Jo, T. P. Russell, A. K. Jen, *Adv. Mater.* **2015**, *27*, 3310 – 3317; j) C. Lee, H. Kang, W. Lee, T. Kim, K. H. Kim, H. Y. Woo, C. Wang, B. J. Kim, *Adv. Mater.* **2015**, *27*, 2466 – 2471; k) L. Ye, X. Jiao, M. Zhou, S. Zhang, H. Yao, W. Zhao, A. Xia, H. Ade, J. Hou, *Adv. Mater.* **2015**, *27*, 6046 – 6054; l) S. Li, H. Zhang, W. Zhao, L. Ye, H. Yao, B. Yang, S. Zhang, J. Hou, *Adv. Energy Mater.* **2016**, *6*, 1501991; m) N. Balar, Y. Xiong, L. Ye, S. Li, D. Nevola, D. B. Dougherty, J. Hou, H. Ade, B. T. O'Connor, *ACS Appl. Mater. Interfaces* **2017**, *9*, 43886 – 43892; n) Y. Li, G. Xu, C. Cui, Y. Li, *Adv. Energy Mater.* **2018**, *8*, 1701791; o) B. T. O'Connor, O. M. Awartani, N. Balar, *MRS Bull.* **2017**, *42*, 108 – 114.

[3] a) Y. Qian, X. Zhang, L. Xie, D. Qi, B. K. Chandran, X. Chen, W. Huang, *Adv. Mater.* **2016**, *28*, 9243 – 9265; b) T. Q. Trung, N. E. Lee, *Adv. Mater.* **2017**, *29*, 1603167; c) G.-J. N. Wang, L. Shaw, J. Xu, T. Kurosawa, B. C. Schroeder, J. Y. Oh, S. J. Benight, Z. Bao, *Adv. Funct. Mater.* **2016**, *26*, 7254 – 7262; d) J.-S. Kim, J.-H. Kim, W. Lee, H. Yu, H. J. Kim, I. Song, M. Shin, J. H. Oh, U. Jeong, T.-S. Kim, B. J. Kim, *Macromolecules* **2015**, *48*, 4339 – 4346; e) J. Y. Oh, S. Rondeau-Gagne, Y. C. Chiu, A. Chortos, F. Lissel, G. N. Wang, B. C. Schroeder, T. Kurosawa, J. Lopez, T. Katsumata, J. Xu, C. Zhu, X. Gu, W. G. Bae, Y. Kim, L. Jin, J. W. Chung, J. B. Tok, Z. Bao, *Nature* **2016**, *539*, 411 – 415.

[4] a) B. Kang, F. Ge, L. Qiu, K. Cho, *Adv. Electron. Mater.* **2017**, *3*, 1600240; b) S. Park, K. Parida, P. S. Lee, *Adv. Energy Mater.* **2017**, *7*, 1701369; c) H.-F. Wen, H.-C. Wu, J. Aimi, C.-C. Hung, Y.-C. Chiang, C.-C. Kuo, W.-C. Chen, *Macromolecules* **2017**, *50*, 4982 – 4992; d) H.-C. Wu, C.-C. Hung, C.-W. Hong, H.-S. Sun, J.-T. Wang, G. Yamashita, T. Higashihara, W.-C. Chen, *Macromolecules* **2016**, *49*, 8540 – 8548; e) X. Zhao, G. Xue, G. Qu, V. Singhania, Y. Zhao, K. Butrouna, A. Gumyusenge, Y. Diao, K. R. Graham, H. Li, J. Mei, *Macromolecules* **2017**, *50*, 6202 – 6209.

[5] a) Y. Wang, C. Zhu, R. Pfattner, H. Yan, L. Jin, S. Chen, F. Molina-Lopez, F. Lissel, J. Liu, N. Rabiah, Z. Chen, J. Chung, C. Linder, M. Toney, B. Murmann, Z. Bao, *Sci. Adv.* **2017**, *3*, e1602076; b) M. Shin, J. Y. Oh, K. E. Byun, Y. J. Lee, B. Kim, H. K. Baik, J. J. Park, U. Jeong, *Adv. Mater.* **2015**, *27*, 1255 – 1261; c) E. Song, B. Kang, H. H. Choi, D. H. Sin, H. Lee, W. H. Lee, K. Cho, *Adv. Electron. Mater.* **2016**, *2*, 1500250; d) H. Kim, J. Byun, S.-H. Bae, T. Ahmed, J.-X. Zhu, S.-J. Kwon, Y. Lee, S.-Y. Min, C. Wolf, H.-K. Seo, J.-H. Ahn, T.-W. Lee, *Adv. Energy Mater.* **2016**, *6*, 1600172; e) K.-G. Lim, S. M. Park, H. Y. Woo, T.-W. Lee, *ChemSusChem* **2015**, *8*, 3062 – 3068.

[6] T. Kumari, M. Moon, S.-H. Kang, C. Yang, *Nano Energy* **2016**, *24*, 56 – 62.

[7] D. Chung, T. G. Kim, *J. Ind. Eng. Chem.* **2007**, *13*, 571 – 577.

[8] a) J. H. Kim, A. Nizami, Y. Hwangbo, B. Jang, H. J. Lee, C. S. Woo, S. Hyun, T. S. Kim, *Nat. Commun.* **2013**, *4*, 2520; b) D. Rodriquez, J. H. Kim, S. E. Root, Z. Fei, P. Boufflet, M. Heeney, T. S. Kim, D. J. Lipomi, *ACS Appl. Mater. Interfaces* **2017**, *9*, 8855 – 8862.

[9] A. D. Scaccabarozzi, N. Stingelin, *J. Mater. Chem. A* **2014**, *2*, 10818 – 10824.

[10] a) H. Hu, P. C. Y. Chow, G. Zhang, T. Ma, J. Liu, G. Yang, H. Yan, *Acc. Chem. Res.* **2017**, *50*, 2519 – 2528; b) H. J. Kim, M. Y. Lee, J. S. Kim, J. H. Kim, H. Yu, H. Yun, K. Liao, T. S. Kim, J. H. Oh, B. J. Kim, *ACS Appl. Mater. Interfaces* **2017**, *9*, 14120 – 14128; c) C. Lu, W. Y. Lee, C. C. Shih, M. Y. Wen, W. C. Chen, *ACS Appl. Mater. Interfaces* **2017**, *9*, 25522 – 25532.

[11] J. R. Tumbleston, B. A. Collins, L. Yang, A. C. Stuart, E. Gann, W. Ma, W. You, H. Ade, *Nat. Photonics* **2014**, *8*, 385 – 391; V. Vohra, K. Kawashima, T. Kakara, T. Koganezawa, I. Osaka, K. Takimiya, H. Murata, *Nat. Photonics* **2015**, *9*, 403 – 408.

[12] J. Rivnay, S. C. Mannsfeld, C. E. Miller, A. Salleo, M. F. Toney, *Chem. Rev.* **2012**, *112*, 5488 – 5519.

[13] a) Y. J. Hwang, T. Earmme, B. A. Courtright, F. N. Eberle, S. A. Jenekhe, *J. Am. Chem. Soc.* **2015**, *137*, 4424 – 4434; b) M. Jeong, S. Chen, S. M. Lee, Z. Wang, Y. Yang, Z. G. Zhang, C. Zhang, M. Xiao, Y. Li, C. Yang, *Adv. Energy Mater.* **2018**, *8*, 1702166; c) D. Han, T. Kumari, S. Jung, Y. An, C. Yang, *Phys. Status Solidi RRL* **2018**, *2*, 1800009; d) S. Chen, H. J. Cho, J. Lee, Y. Yang, Z. G. Zhang, Y. Li, C. Yang, *Adv. Energy Mater.* **2017**, *7*, 1701125; e) T. Kumari, S. M. Lee, K. C. Lee, Y. Cho, C. Yang, *Adv. Energy Mater.* **2018**, *8*, 1800616; f) Y. An, J. Oh, S. Chen, B. Lee, S. M. Lee, D. Han, C. Yang, *Polym. Chem.* **2018**, *9*, 593 – 602; g) Z. Li, X. Xu, W. Zhang, X. Meng, W. Ma, A. Yartsev, O. Inganas, M. R.

Andersson, R. A. Janssen, E. Wang, *J. Am. Chem. Soc.* **2016**, *138*, 10935 – 10944.
[14] a) X. Guo, N. Zhou, S. J. Lou, J. Smith, D. B. Tice, J. W. Hennek, R. P. Ortiz, J. T. L. Navarrete, S. Li, J. Strzalka, L. X. Chen, R. P. H. Chang, A. Facchetti, T. J. Marks, *Nat. Photonics* **2013**, *7*, 825 – 833; b) D. Bartesaghi, C. Perez Idel, J. Kniepert, S. Roland, M. Turbiez, D. Neher, L. J. Koster, *Nat. Commun.* **2015**, *6*, 7083.
[15] S. R. Cowan, A. Roy, A. J. Heeger, *Phys. Rev. B* **2010**, *82*, 245207 – 245216.
[16] P. W. M. Blom, M. J. M. de Jong, M. G. van Munster, *Phys. Rev. B* **1997**, *55*, R656 – R689.
[17] a) S. Jung, J. Lee, J. Seo, U. Kim, Y. Choi, H. Park, *Nano Lett.* **2018**, *18*, 1337 – 1343; b) S. Jung, J. Lee, Y. Choi, S. M. Lee, C. Yang, H. Park, *2D Mater.* **2017**, *4*, 045004.
[18] a) K. P. Loh, S. W. Tong, J. Wu, *J. Am. Chem. Soc.* **2016**, *138*, 1095 – 1102; b) A. Pirkle, J. Chan, A. Venugopal, D. Hinojos, C. W. Magnuson, S. McDonnell, L. Colombo, E. M. Vogel, R. S. Ruoff, R. M. Wallace, *Appl. Phys. Lett.* **2011**, *99*, 122108.

Manuscript received: June 30, 2018
Revised manuscript received: August 1, 2018
Accepted manuscript online: August 16, 2018
Version of record online: September 4, 2018

